Journal of Computational Physics 228 (2009) 7215–7232

Contents lists available at ScienceDirect

Journal of Computational Physics

journal homepage: www.elsevier.com/locate/jcp

Mimetic finite difference method for the Stokes problem on polygonal meshes

L. Beirão da Veiga [a], V. Gyrya [b,*], K. Lipnikov [c], G. Manzini [d]

[a] Dipartimento di Matematica "F.Enriques", Via Saldini 50, 20133 Milano, Italy
[b] The Pennsylvania State University, Department of Mathematics, University Park, PA 16802, USA
[c] Los Alamos National Laboratory, MS B284, Los Alamos, NM 87545, USA
[d] Istituto di Matematica Applicata e Tecnologie Informatiche-CNR, Via Ferrata 1, 27100 Pavia, Italy

ARTICLE INFO

Article history:
Received 25 December 2008
Received in revised form 17 June 2009
Accepted 18 June 2009
Available online 3 July 2009

Keywords:
Incompressible Stokes equations
Mimetic discretization
Polygonal mesh

ABSTRACT

Various approaches to extend finite element methods to non-traditional elements (general polygons, pyramids, polyhedra, etc.) have been developed over the last decade. The construction of basis functions for such elements is a challenging task and may require extensive geometrical analysis. The mimetic finite difference (MFD) method works on general polygonal meshes and has many similarities with low-order finite element methods. Both schemes try to preserve the fundamental properties of the underlying physical and mathematical models. The essential difference between the two schemes is that the MFD method uses only the surface representation of discrete unknowns to build the stiffness and mass matrices. Since no extension of basis functions inside the mesh elements is required, practical implementation of the MFD method is simple for polygonal meshes that may include degenerate and non-convex elements. In this article, we present a new MFD method for the Stokes problem on arbitrary polygonal meshes and analyze its stability. The method is developed for the general case of tensor coefficients, which allows us to apply it to a linear elasticity problem, as well. Numerical experiments show, for the velocity variable, second-order convergence in a discrete L^2 norm and first-order convergence in a discrete H^1 norm. For the pressure variable, first-order convergence is shown in the L^2 norm.

1. Introduction

Stokes flow is a type of fluid flow where advective inertial forces are small compared with viscous forces. Mathematically, such flows are characterized by a very small Reynolds number, which is typical for microscale problems, where the velocities and sizes of objects are small. Stokes flow is a good approximation for a number of important physical problems, such as sedimentation, bio-suspensions, the construction of efficient fibrous filters and the development of energy efficient micro-fluidic devices (e.g. mixers).

Finite element (FE) methods form a popular class of methods for computing Stokes flows numerically. Traditionally, FE methods rely on triangular (simplicial) and quadrilateral meshes. But in complex simulations one often encounters general polygonal and polyhedral meshes (see e.g. [22]). In some cases these meshes are more efficient in partitioning the computational domain. In other cases they are given as an entry point to the problem (e.g. by a data collection agent or a

* Corresponding author. Tel.: +1 973 865 1226.
E-mail addresses: beirao@mat.unimi.it (L. Beirão da Veiga), gyrya@math.psu.edu (V. Gyrya), lipnikov@lanl.gov (K. Lipnikov), Marco.Manzini@imati.cnr.it (G. Manzini).

0021-9991/$ - see front matter © 2009 Elsevier Inc. All rights reserved.
doi:10.1016/j.jcp.2009.06.034

multi-physics solver routine). The polygonal meshes can be sufficiently general. For instance, Lagrangian meshes may result in non-convex elements due to specifics of the flow dynamics. In the geosciences, the termination by thinning of a geological layer is sometimes modeled by degenerate hexahedra with multiple vertices having the same coordinates. In the process of constructing adaptive solutions of PDEs on quadrilateral and hexahedral meshes, local refinement of the mesh creates degenerate elements that have 180° angles between faces. These issues motivate the development of discretization methods suited to general polygonal and polyhedral meshes.

Various approaches to extend the FE methods to non-traditional elements (pyramids, polyhedra, etc.) have been developed over the last decade (see, e.g. [25,29,30,35,36]). The main challenge for these methods is the construction of basis functions for a general polygonal element. This often requires extensive geometrical analysis. For instance, in [29] an auxiliary simplicial partition is used in each polygonal element to simplify the construction of FE basis functions for this element.

MFD methods [33,13,15,14,11] combine the analytical power of FE methods with the flexibility provided by polygonal and polyhedral meshes. Both methods try to preserve the fundamental properties of physical and mathematical models such as conservation laws, solution symmetries and positivity and the fundamental identities and theorems of vector and tensor calculus (e.g. Green's identities). Contrary to the FE methods, the MFD methods use only a surface representation of the discrete unknowns to build the stiffness and mass matrices. Since no extension inside the mesh element is required, practical implementation of MFD methods is simple for polygonal and polyhedral meshes.

MFD methods have been successfully employed for solving diffusion [11,14,27], convection–diffusion [18], electromagnetic [27] and elasticity [2] problems and for modeling fluid flows [1,16,31]. The original MFD methods were low-order methods. Miscellaneous approaches were developed to build higher-order methods [32,6,26,4].

A posteriori error estimates are an important part of the development of MFD methods. A local error estimator for the diffusion problem is presented, analyzed and tested in [3,8], while in [17] a post-processing methodology is introduced. Finally, we mention a few relevant finite volume discretization methods on polygonal and polyhedral meshes (see [20,23] and references therein) which, similar to the FE and MFD methods, are designed to preserve important properties of continuum equations.

In this paper we present a new MFD method for the Stokes problem on polygonal meshes. The derivation of the new method is based on the methodology proposed originally in [15] for diffusion problems. The formulation of the Stokes problem involves a tensor viscosity coefficient so that the developed method may also be used to solve linear elasticity problems in the displacement formulation. Note that a mixed stress–displacement formulation of the elasticity problem is developed in [2].

The developed MFD method is first-order accurate for the fluid velocity in a discrete H^1 norm and for the pressure in the L^2 norm. In addition, whenever the coefficients of the fluid viscosity tensor are piecewise constant, the method results in second-order convergence for the velocity variable in a discrete L^2 norm. Note that we build a whole family of methods with equivalent properties. For instance, on triangular meshes our family of methods contains the reduced $P_2 - P_0$ finite element method [24,9]. A detailed convergence analysis of this family and the extension to three dimensions will be the topic for future research [5].

The proposed MFD method belongs to the class of staggered mesh methods; the velocity unknowns are defined at mesh vertices and on mesh edges while the pressure unknowns are defined on mesh elements. Other staggered discretizations for Stokes and linear elasticity include a huge body of various FE and FV methods (see e.g. [24,9,12,21,10] and references therein).

The paper is organized as follows. In Section 2, we discuss the variational form of the Stokes problem. In Section 3, we present the new MFD method. In Section 4, we analyze the stability of the discretization. In Section 5, we illustrate the proposed method with three numerical experiments.

2. Variational formulation for the Stokes equation

Let Ω be a polygonal domain with Lipschitz continuous boundary $\partial\Omega$. Let us consider the incompressible Stokes equation

$$\begin{cases} -2\mathrm{div}(\nu D(\mathbf{u})) = \mathbf{F} - \nabla p \\ \mathrm{div}(\mathbf{u}) = 0 \end{cases} \quad \text{in } \Omega, \tag{1}$$

where $\mathbf{u}$ is the fluid velocity, p is the pressure, $\mathbf{F}$ is a given external force (e.g. gravity), ν is a fourth-order symmetric positive definite *tensor* fluid viscosity,

$$\nu_{klnm} = \nu_{lknm} = \nu_{nmkl} = \nu_{mnkl}, \tag{2}$$

and $D(\mathbf{u})$ is the symmetrized gradient,

$$2D(\mathbf{u}) = \nabla\mathbf{u} + (\nabla\mathbf{u})^T.$$

We impose Dirichlet boundary conditions on $\Gamma_D \subset \partial\Omega$ and Neumann boundary conditions on $\Gamma_N = \partial\Omega \setminus \Gamma_D$ (both Γ_D and Γ_N are a finite union of connected components)

$$\begin{aligned} &\mathbf{u}(\mathbf{x}) = \mathbf{g}(\mathbf{x}) \quad \text{for } \mathbf{x} \in \Gamma_D, \\ &\sigma(\mathbf{u}(\mathbf{x}), p(\mathbf{x}))\mathbf{n}(\mathbf{x}) = \mathbf{h}(\mathbf{x}) \quad \text{for } \mathbf{x} \in \Gamma_N, \end{aligned} \tag{3}$$

where σ is the stress tensor,

$$\sigma(\mathbf{u}, p) = 2\nu D(\mathbf{u}) - pI.$$

Remark 1. For simplicity, we assume that the measure of Γ_D is positive, in order to have the uniqueness of the vector variable $\mathbf{u}$. Furthermore, note that, in the case $\Gamma_D = \partial\Omega$,

- the pressure variable is defined up to a global constant and
- the boundary datum must be consistent with the incompressibility condition, i.e.

$$\int_{\partial\Omega} \mathbf{g}\cdot\mathbf{n}\, d\mathbf{x} = 0,$$

where $\mathbf{n}$ is the unit outward normal to $\partial\Omega$.

Next, we derive a variational formulation for problem (1)–(3). The class $X_{\mathbf{g}}$ of admissible velocity fields $\mathbf{u}$ is defined by

$$X_{\mathbf{g}} := \{\mathbf{u} \in X : \ \mathbf{u}(\mathbf{x}) = \mathbf{g}(\mathbf{x}) \quad \text{for } \mathbf{x} \in \Gamma_D\}, \tag{4}$$

where $X := (H^1(\Omega))^2$. We do not require that the functions in $X_{\mathbf{g}}$ be incompressible (incompressibility is enforced by an additional constraint). We will also need a linear space X_0 of variations in the admissible class $X_{\mathbf{g}}$. It is defined by setting $\mathbf{g} = 0$ in (4).

Multiplying the first equation in (1) by a test function $\mathbf{v} \in X_0$, integrating by parts over Ω and using boundary conditions (3) yield

$$2\int_\Omega \nu D(\mathbf{u}) : \nabla\mathbf{v}\, d\mathbf{x} - \int_\Omega p\,\mathrm{div}(\mathbf{v})\ d\mathbf{x} = \int_\Omega \mathbf{F}\cdot\mathbf{v}\, d\mathbf{x} + \int_{\Gamma_N} \mathbf{h}\cdot\mathbf{v}\, d\mathbf{x} \quad \forall\mathbf{v} \in X_0. \tag{5}$$

Let us introduce the following notation:

$$\mathcal{A}(\mathbf{u}, \mathbf{v}) := \int_\Omega (2\nu D(\mathbf{u})) : D\mathbf{v}\ d\mathbf{x}, \tag{6}$$

$$\mathcal{B}(p, \mathbf{v}) := \int_\Omega p\,\mathrm{div}(\mathbf{v})\ d\mathbf{x}, \tag{7}$$

$$\mathcal{L}(\mathbf{v}) := \int_\Omega \mathbf{F}\cdot\mathbf{v}\ d\mathbf{x} + \int_{\Gamma_N} \mathbf{h}\cdot\mathbf{v}\ d\mathbf{x}. \tag{8}$$

Note that the bilinear form $\mathcal{A}(\mathbf{u}, \mathbf{v})$ is symmetric since $\nabla\mathbf{v}$ can be replaced with $D(\mathbf{v})$, due to (2). In such a notation, Eq. (5) takes the following form

$$\mathcal{A}(\mathbf{u}, \mathbf{v}) - \mathcal{B}(p, \mathbf{v}) = \mathcal{L}(\mathbf{v}). \tag{9}$$

Now we multiply the incompressibility equation in (1) by $q \in L^2(\Omega)$ and integrate over the domain Ω to get the variational formulation:

Find a pair $(\mathbf{u}, p), \mathbf{u} \in X_{\mathbf{g}}$ *and* $p \in L^2(\Omega)$, *such that*

$$\begin{cases} \mathcal{A}(\mathbf{u}, \mathbf{v}) - \mathcal{B}(p, \mathbf{v}) = \mathcal{L}(\mathbf{v}) & \forall\mathbf{v} \in X_0, \\ \mathcal{B}(q, \mathbf{u}) = 0 & \forall q \in L^2(\Omega). \end{cases} \tag{10}$$

3. Discretization on polygons

Let Ω^h be a partition of the computational domain Ω into $\mathcal{N}(\Omega^h)$ polygons E. We assume that this partition is conformal, i.e. intersection of two different elements E_1 and E_2 is either a few mesh points, or a few mesh edges (two adjacent elements may share more than one edge) or empty. We allow Ω^h to contain non-convex and degenerate elements. We approximate the coefficient ν by a constant tensor inside each mesh element. The extension to the case of a tensor with variable coefficients will be studied in the future using the ideas developed for diffusion problems in [4].

Let us briefly describe the formal construction of our mimetic discretization. Note that the numerical approximation to problem (10) requires to discretize scalar and vector functions, which are, respectively, elements of $L^2(\Omega)$ and $(H^1(\Omega))^2$, the bilinear forms $\mathcal{A}(\mathbf{u}, \mathbf{v})$ and $\mathcal{B}(p, \mathbf{v})$, and the linear functional $\mathcal{L}(\mathbf{v})$.

We begin by introducing the degrees of freedom for scalar and vector functions

$$\begin{aligned} &p, s \in L^2(\Omega) \ \rightarrow\ P, S \in Q^h, \\ &\mathbf{u}, \mathbf{v} \in H^1(\Omega) \ \rightarrow\ U, V \in X^h, \end{aligned} \tag{11}$$

that are used to discretize the bilinear forms and the linear functional mentioned above as follows

$$\begin{aligned} \mathcal{A}(\mathbf{u},\mathbf{v}) &\rightarrow V^T\mathbf{A}U, \\ \mathcal{B}(p,\mathbf{v}) &\rightarrow V^T\mathbf{D}^T P, \\ \mathcal{L}(\mathbf{v}) &\rightarrow V^T L. \end{aligned} \tag{12}$$

Here, we anticipate that $\mathbf{A}$ is a symmetric semi-definite matrix with three null modes corresponding to the rigid body motions, one for rotation and two for translations.

These characteristics are directly exploited in the algorithm used to compute this matrix. The details of the construction of $\mathbf{A}$, $\mathbf{D}$ and L are presented in the following subsections.

Let $X^h_{\mathbf{g}}$ and X^h_0 denote the subsets of X^h that approximate $X_{\mathbf{g}}$ and X_0, respectively. Our new mimetic discretization for the Stokes problem reads as follows.

Find $U \in X^h_{\mathbf{g}}$ and $P \in Q^h$, such that

$$\begin{aligned} &V^T\mathbf{A}U - V^T\mathbf{D}^T P = V^T L \quad \forall V \in X^h_0, \\ &U^T\mathbf{D}^T S = 0 \quad \forall S \in Q^h. \end{aligned}$$

This problem can be written in the matrix form:

$$\begin{bmatrix} V \\ S \end{bmatrix}^T \begin{bmatrix} \mathbf{A} & -\mathbf{D}^T \\ -\mathbf{D} & 0 \end{bmatrix} \begin{bmatrix} U \\ P \end{bmatrix} = \begin{bmatrix} V^T L \\ 0 \end{bmatrix} \quad \forall V \in X^h_0 \text{ and } \forall S \in Q^h. \tag{13}$$

In practice, we find it convenient to eliminate the degrees of freedom corresponding to the Dirichlet boundary conditions, c.f. Section 3.5. This results in the saddle point problem:

$$\begin{bmatrix} \mathbf{A}_0 & -\mathbf{D}_0^T \\ -\mathbf{D}_0 & 0 \end{bmatrix} \begin{bmatrix} U_0 \\ P \end{bmatrix} = \begin{bmatrix} G_U \\ G_P \end{bmatrix}, \tag{14}$$

where $\mathbf{A}_0$ and $\mathbf{D}_0$ are sub-matrices of $\mathbf{A}$ and $\mathbf{D}$, respectively. Note that matrix $\mathbf{A}_0$ is symmetric and positive definite. Therefore, a number of efficient iterative solvers, such as the preconditioned Lanzcos algorithm or other Krylov methods, are available from the literature to solve problem (14).

3.1. Discretization of scalar and vector functions

Let us consider the sample element E shown in Fig. 1. We denote the number of its vertices by $\mathcal{N}(E)$. Note that the number of its edges is also $\mathcal{N}(E)$. Let $\mathbf{n}_E(\mathbf{x})$ be the unit outward normal to the boundary ∂E at the point $\mathbf{x}$.

For scalar functions (e.g. pressure p), we specify one degree of freedom per element, p_E. For instance, p_E may be the average value of p over the element E. The local approximation space Q_E has dimension one and is isomorphic to the space of constant functions on E. The dimension of the global space Q^h is equal to the number of mesh elements $\mathcal{N}(\Omega^h)$.

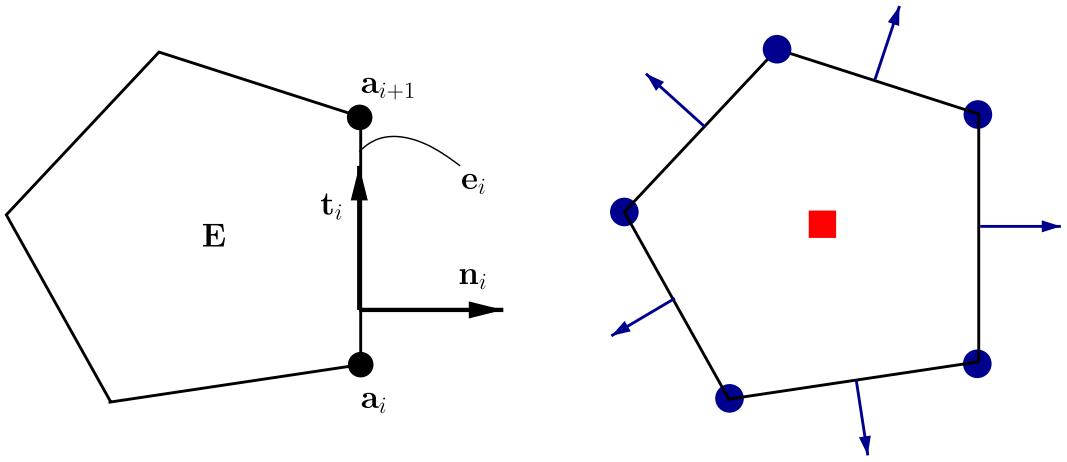

Fig. 1. Left picture introduces notations used through the paper. Right picture shows the degrees of freedom for pressure (square box) and velocity (circles and arrows).

Let us specify the degrees of freedom for vector functions such as the velocity $\mathbf{u}$. To each vertex $\mathbf{a}_i$ of a polygonal element E, we assign two degrees of freedom that represent the *value* of $\mathbf{u}$ at $\mathbf{a}_i$:

$$\left(U_i^x, U_i^y\right)^T := \mathbf{u}(\mathbf{a}_i), \quad i = 1, \ldots, \mathcal{N}(E).$$

To each edge e_i of E, we assign one degree of freedom that represents the *average flux* of $\mathbf{u}$ through the edge:

$$U_i^e := \frac{1}{|e_i|} \int_{e_i} \mathbf{u}(s) \cdot \mathbf{n}_i \, ds, \tag{15}$$

where $\mathbf{n}_i$ is the restriction of $\mathbf{n}_E(\mathbf{x})$ to edge e_i.

The local space X_E^h is characterized by $\mathcal{D}(E) := 3\mathcal{N}(E)$ degrees of freedom for each polygonal element E. The dimension of the global space X^h is the number of mesh edges plus twice the number of mesh vertices. The dimensions of both spaces $X_{\mathbf{g}}^h$ and X_0^h is equal to the dimension of X^h minus the number of Dirichlet edges and minus twice the number of Dirichlet points.

Let U_E be the restriction of $U \in X^h$ to the element E,

$$U_E = \left(U_1^x, U_1^y, U_1^e, U_2^x, U_2^y, U_2^e, \ldots, U_{\mathcal{N}(E)}^x, U_{\mathcal{N}(E)}^y, U_{\mathcal{N}(E)}^e\right)^T. \tag{16}$$

In the next subsection, we will show that the space X_E^h is isomorphic to a specially designed space $\mathcal{V}_E$ of vector functions. In other words, for every U_E in X_E^h, there exists a *unique* vector function $\mathbf{u}_E$ in a certain approximation space $\mathcal{V}_E$ that we will discuss in detail in Section 3.2.1. Note that X_E^h is also isomorphic to $\mathbb{R}^{\mathcal{D}(E)}$, the linear space of real vectors of size $\mathcal{D}(E)$.

3.2. Discretization of $\mathcal{A}(\mathbf{u}, \mathbf{v})$

We reduce the discretization of the global bilinear form $\mathcal{A}(\mathbf{u}, \mathbf{v})$ to the discretization of the elemental bilinear forms $\mathcal{A}_E(\mathbf{u}_E, \mathbf{v}_E)$ which are defined for the elemental restrictions $\mathbf{u}_E, \mathbf{v}_E$ in $\mathcal{V}_E$:

$$\mathcal{A}(\mathbf{u}, \mathbf{v}) := \sum_{E \in \Omega_h} \mathcal{A}_E(\mathbf{u}_E, \mathbf{v}_E). \tag{17}$$

We remark that the decomposition in (17) is the usual assembly of the stiffness matrix in finite element methods. Let $U_E, V_E \in X_E^h$ be the vector representations of $\mathbf{u}_E, \mathbf{v}_E \in \mathcal{V}_E$. Then,

$$U_E^T \mathbf{A}_E V_E := \mathcal{A}_E(\mathbf{u}_E, \mathbf{v}_E) = \int_E 2\nu D(\mathbf{u}_E) : D(\mathbf{v}_E) \, d\mathbf{x}.$$

The goal of this subsection is to present our new mimetic strategy for the calculation of the elemental matrices $\mathbf{A}_E$. To this purpose, we first discuss the derivation of a computable form of $\mathbf{A}_E$, which is based on a block-diagonalization of this matrix. Then, we propose an alternative but equivalent formulation that is easier to implement and computationally less expensive.

3.2.1. Divide and conquer strategy

So far, we have roughly followed the finite element setting. In such a framework, the next step would be the introduction of a set of basis functions defined on each element E or, possibly, on a reference element $\widehat{E}$. However, this step would be quite challenging for a polygonal element E that has a general shape.

To avoid this problem, we use a different approach that is based on the following linear algebraic argument.

Let the columns of the square matrix $\mathbf{T}_E$ form a new basis in X_E^h. Then, the elemental stiffness matrix is transformed as follows:

$$\widetilde{\mathbf{A}}_E := \mathbf{T}_E^T \mathbf{A}_E \mathbf{T}_E. \tag{18}$$

In Section 3.2.2, we shall *explicitly* construct a transformation matrix $\mathbf{T}_E$ such that matrix $\widetilde{\mathbf{A}}_E$ is block-diagonal and takes the form

$$\widetilde{\mathbf{A}}_E = \begin{bmatrix} \widetilde{\mathbf{A}}_E^{11} & 0 \\ 0 & \widetilde{\mathbf{A}}_E^{22} \end{bmatrix}, \tag{19}$$

where sub-matrix $\widetilde{\mathbf{A}}_E^{11}$ is *computable* and sub-matrix $\widetilde{\mathbf{A}_E^{22}}$ is an *arbitrary* symmetric and positive definite matrix that scales like $\tilde{\mathbf{A}}_E^{11}$ with respect to the element size and ν. After such block-diagonal matrices are set, matrix $\mathbf{A}_E$ can be calculated as $\mathbf{A}_E = \mathbf{T}_E^{-T} \tilde{\mathbf{A}}_E \mathbf{T}_E^{-1}$. An alternative but more efficient implementation is also described in Section 3.2.4.

The keys to the block-diagonal structure (19) are (i) a carefully selected decomposition of the approximation space,

$$\mathcal{V}_E := \mathcal{V}_{E,1} \oplus \mathcal{V}_{E,2}, \tag{20}$$

where $\mathcal{V}_{E,1}$ and $\mathcal{V}_{E,2}$ are $\mathcal{A}_E$-orthogonal, and (ii) the $\mathcal{P}_1$-compatibility property that will be introduced in Section 3.2.2.

We define $\mathcal{V}_{E,1}$ as the space of linear vector functions over the element E, i.e. $\mathcal{V}_{E,1} := (\mathcal{P}_1(E))^2$. This choice allows us to obtain a numerical scheme that is consistent with all linear vector fields, a crucial property to achieve second-order

convergence. On its turn, space $\mathcal{V}_{E,2}$ will be defined only partially in accordance with the fact that matrix $\widetilde{\mathbf{A}}_E^{22}$ can be arbitrarily chosen. This freedom results in a family of methods, all of whose members show equivalent approximation properties.

Let $\{\boldsymbol{\phi}_i\}_{i=1}^{\mathcal{D}(E)}$ be the set of basis functions that we consider in $\mathcal{V}_E$.

- The first six members of this set are given by:

$$\begin{aligned} \boldsymbol{\phi}_1(x,y) &:= \begin{bmatrix} 1 \\ 0 \end{bmatrix}, \quad \boldsymbol{\phi}_2(x,y) := \frac{1}{2}\begin{bmatrix} y \\ -x \end{bmatrix}, \quad \boldsymbol{\phi}_3(x,y) := \begin{bmatrix} 0 \\ 1 \end{bmatrix}, \\ \boldsymbol{\phi}_4(x,y) &:= \begin{bmatrix} x \\ 0 \end{bmatrix}, \quad \boldsymbol{\phi}_5(x,y) := \frac{1}{2}\begin{bmatrix} y \\ x \end{bmatrix}, \quad \boldsymbol{\phi}_6(x,y) := \begin{bmatrix} 0 \\ y \end{bmatrix}, \end{aligned} \tag{21}$$

and form a basis for the subspace $\mathcal{V}_{E,1}$. Note that $\boldsymbol{\phi}_1, \boldsymbol{\phi}_2, \boldsymbol{\phi}_3$ span the entire space of rigid body motions, while $\boldsymbol{\phi}_1$ and $\boldsymbol{\phi}_3$ alone span the space of translations.

- The functions $\boldsymbol{\phi}_j$ for $j = 7, \ldots, \mathcal{D}(E)$ form a basis for the subspace $\mathcal{V}_{E,2}$ and are chosen $\mathcal{A}_E$-orthogonal to $\mathcal{V}_{E,1}$, in order to obtain the block-diagonal form shown in (19). Thus, there holds that

$$\mathcal{A}_E(\boldsymbol{\phi}_i, \boldsymbol{\phi}_j) = 0, \quad 1 \leqslant i \leqslant 6 < j \leqslant \mathcal{D}(E). \tag{22}$$

Note that the basis functions $\boldsymbol{\phi}_j$ for $j = 7, \ldots, \mathcal{D}(E)$ are to be defined only on the edges of E. This fact will allow us to rewrite orthogonality condition (22) in a computable form, as pointed out in Section 3.2.3.

3.2.2. $\mathcal{P}_1$-compatibility property

Let E denote an element of the mesh, ν be the constant tensor that approximates the fluid viscosity tensor on E and $\mathbf{u}_1$ be a vector field that belongs to $\mathcal{V}_{E,1}$. We state the $\mathcal{P}_1$-compatibility property as

$$\int_E \nu D(\mathbf{u}_1) : D(\mathbf{v}_E)\, d\mathbf{x} = \int_{\partial E} (\nu D(\mathbf{u}_1) \cdot \mathbf{n}_E) \cdot \mathbf{v}_E\, ds \quad \forall \mathbf{v}_E \in \mathcal{V}_E. \tag{23}$$

Identity (23) corresponds to an integration by parts and is the only consistency-type property that we require in the formulation of the scalar product expressed by $\mathcal{A}_E$. As a consequence, this property implies that the calculation of the stiffness matrix $\mathbf{A}_E$ only requires to know $\mathbf{v}_E$ on the edges of E. We make two additional assumptions on the approximation space $\mathcal{V}_E$. Let e_i be the edge of element E with vertices $\mathbf{a}_i$ and $\mathbf{a}_{i+1}$, c.f. Fig. 1. Then,

(A1) the restriction of $\mathbf{v}_E \cdot \mathbf{n}_E$ to e_i, which is the normal component of $\mathbf{v}_E$ along edge e_i, is the quadratic function of the position that is uniquely determined by the degrees of freedom at $\mathbf{a}_i$ and $\mathbf{a}_{i+1}$ and the flux degree-of-freedom V_i^e;

(A2) the restriction of $\mathbf{v}_E \cdot \mathbf{t}_E$ to e_i, which is the tangential component of $\mathbf{v}_E$ along edge e_i, is the linear function of the position which is uniquely determined by the velocity degrees of freedom at the vertices $\mathbf{a}_i$ and $\mathbf{a}_{i+1}$.

These conditions imply the continuity of the discrete velocity across all mesh edges. Moreover, using the notation of Fig. 1 and assumption **(A2)**, we immediately have the following representation of the boundary integrals in (23) in terms of the discrete degrees of freedom:

$$\begin{aligned} \int_{e_i} (2\nu D(\mathbf{u}_1) \cdot \mathbf{n}_i) \cdot \mathbf{v}_E\, ds &= \int_{e_i} (\mathbf{c} \cdot \mathbf{n}_i)(\mathbf{v}_E \cdot \mathbf{n}_i)\, ds + \int_{e_i} (\mathbf{c} \cdot \mathbf{t}_i)(\mathbf{v}_E \cdot \mathbf{t}_i)\, ds \\ &= (\mathbf{c} \cdot \mathbf{n}_i)|e_i| V_i^e + (\mathbf{c} \cdot \mathbf{t}_i)\frac{|e_i|}{2}\left(V_i^x + V_{i+1}^x,\ V_i^y + V_{i+1}^y\right)^T \cdot \mathbf{t}_i, \end{aligned} \tag{24}$$

where we have set $\mathbf{c} = 2\nu D(\mathbf{u}_1)$ to ease notation, and $\mathbf{t}_i$ is the unit vector parallel to e_i.

3.2.3. Change of basis in X_E^h

Let $\mathbf{T}_E$ be the transformation matrix that acts from the basis set $\{\boldsymbol{\phi}_i\}_i$ to the natural basis of X_E^h, this latter being the basis directly associated to the degrees of freedom. Hence,

$$\mathbf{T}_E = \{T_{E,ij}\}, \quad T_{E,ij} := i\text{-th degree of freedom of } \boldsymbol{\phi}_j. \tag{25}$$

The first six columns of $\mathbf{T}_E$ are uniquely determined by the choice of the basis functions (21).

For example, in accordance with the definition of the vector degrees of freedom given in (16), the column vectors T_j for $j = 1, \ldots, 6$ are given by

$$T_j = \left((\boldsymbol{\phi}_j(x_1,y_1))^x, (\boldsymbol{\phi}_j(x_1,y_1))^y, (\boldsymbol{\phi}_j)_1^e, (\boldsymbol{\phi}_j(x_2,y_2))^x, (\boldsymbol{\phi}_j(x_2,y_2))^y, (\boldsymbol{\phi}_j)_2^e, \ldots (\boldsymbol{\phi}_j(x_{\mathcal{N}(E)},y_{\mathcal{N}(E)}))^x, (\boldsymbol{\phi}_j(x_{\mathcal{N}(E)},y_{\mathcal{N}(E)}))^y, (\boldsymbol{\phi}_j)_{\mathcal{N}(E)}^e \right)^T,$$

where $(\boldsymbol{\phi}_j(x_k,y_k))^x$ and $(\boldsymbol{\phi}_j(x_k,y_k))^y$ are the first and second components of the j-th basis function calculated at the k-th node, c.f. Eq. (21), and $(\boldsymbol{\phi}_j)^e$ is the edge integral (15).

The remaining columns T_j for $j > 6$ are obtained by imposing the $\mathcal{A}_E$-orthogonality, c.f. Eq. (22), and the $\mathcal{P}_1$-compatibility property, c.f. Eq. (23).

To this purpose, we introduce the auxiliary vectors $R(\phi_i), i = 1, \ldots, 6$, in $\mathbb{R}^{\mathcal{D}(E)}$, which are such that

$$R(\phi_i)^T V_E = \int_{\partial E} (vD(\phi_i) \cdot \mathbf{n}_E) \cdot \mathbf{v}_E \, ds \quad \forall V_E \in X_E^h. \tag{26}$$

The j-th entry of the column vector $R(\phi_i)$ can be readily calculated by splitting the right-hand side integral of (26) into the sum of all edge contributions and applying (24) to vector V_E (and to the corresponding vector field $\mathbf{v}_E$) that runs through the canonical basis vectors of $\mathbb{R}^{\mathcal{D}(E)}$. As already observed after Eq. (21), the first three basis functions ϕ_1, ϕ_2 and ϕ_3, in $\mathcal{V}_E$ correspond to the rigid body motions. Therefore, $R(\phi_1) = R(\phi_2) = R(\phi_3) = 0$, and only $R(\phi_j)$ for $j = 4, 5, 6$ must be explicitly computed.

Since V_E is arbitrary, the $\mathcal{P}_1$-compatibility property (23) gives

$$T_i^T \mathbf{A}_E = R(\phi_i)^T, \quad 1 \leqslant i \leqslant 6, \tag{27}$$

which makes it possible to rewrite orthogonality condition (22) as:

$$0 = \mathcal{A}_E(\phi_i, \phi_j) = R(\phi_i)^T T_j, \quad 1 \leqslant i \leqslant 6 < j \leqslant \mathcal{D}(E). \tag{28}$$

Relation (28) provides only three conditions for the index values $i = 4, 5, 6$, because $R(\phi_i) = 0$ for $i = 1, 2, 3$, while we have to define $\mathcal{D}(E) - 6$ basis vectors in X_E^h. To recover three additional conditions, we impose that

$$T_i^T T_j = 0 \quad 1 \leqslant i \leqslant 3 \text{ and } 6 < j \leqslant \mathcal{D}(E). \tag{29}$$

Conditions (28) and (29) can be either imposed in a direct way through the Gram-Schmidt or the SVD orthogonalization algorithms, or, as proposed in Section 3.2.4, through an orthogonal projection.

We now introduce a more compact notation, which will be useful here and in the analysis of Section 4. Let $\mathbf{T}_{i..j}$ be the $\mathcal{D}(E) \times (j - i + 1)$ matrix given by selecting the columns $i, \ldots, j$ from $\mathbf{T}_E$:

$$\mathbf{T}_{i..j} = [T_i, T_{i+1}, \ldots, T_j].$$

Hereafter, to simplify the notation, we shall also write $\mathcal{D}$ instead of $\mathcal{D}(E)$. Using this notation, we may write $\mathbf{T}_{1..\mathcal{D}}$ instead of $\mathbf{T}_E$. We introduce a similar notation for the matrices $\mathbf{R}_{i..j}$, which are formed by the vectors $R_i = R(\phi_i)$ for $i = 1, \ldots, 6$. Let us define $\mathbf{R}_E := \mathbf{R}_{1..6}$ and summarize all the relations discussed so far:

$$\mathbf{R}_{1..3} = \mathbf{0}, \tag{30}$$

$$\mathbf{A}_E \mathbf{T}_{1..6} = \mathbf{R}_E, \tag{31}$$

$$\mathbf{A}_E^{11} := \mathbf{T}_{1..6}^T \mathbf{A}_E \mathbf{T}_{1..6} = \mathbf{T}_{1..6}^T \mathbf{R}_E, \tag{32}$$

$$\mathbf{T}_{7..\mathcal{D}}^T \mathbf{A}_E \mathbf{T}_{1..6} = \mathbf{T}_{7..\mathcal{D}}^T \mathbf{R}_E = \mathbf{0}, \tag{33}$$

$$\mathbf{T}_{7..\mathcal{D}}^T \mathbf{T}_{1..3} = \mathbf{0}. \tag{34}$$

Observe that the last $(\mathcal{D} - 6)$ columns of $\mathbf{T}_E$ can still be chosen mutually orthogonal and can be scaled arbitrarily. It will be convenient to assume that

$$\mathbf{T}_{7..\mathcal{D}}^T \mathbf{T}_{7..\mathcal{D}} = |E| \mathbf{I}_{\mathcal{D}-6}, \tag{35}$$

where $\mathbf{I}_{\mathcal{D}-6}$ represents the identity matrix of size $(\mathcal{D} - 6)$. The columns of the basis transformation matrix $\mathbf{T}_E$ are $\mathcal{D}$ linearly independent vectors in $\mathbb{R}^{\mathcal{D}}$ thus ensuring that this matrix is non singular. This property is a direct consequence of the matrix construction and is formally proven in the final lemma presented at the end of this subsection.

We are now left with the problem of constructing the matrix $\widetilde{\mathbf{A}}_E^{11}$ and choosing the proper matrix $\widetilde{\mathbf{A}}_E^{22}$. The entries of the 6×6 symmetric matrix $\widetilde{\mathbf{A}}_E^{11}$, defined by (32), can be computed directly using the basis functions (21) from formula (23). Moreover, (30) implies that the corresponding entries of matrix $\widetilde{\mathbf{A}}_E^{11}$ are zero, so that we obtain the 2×2 block decomposition form

$$\widetilde{\mathbf{A}}_E^{11} = \begin{bmatrix} 0 & 0 \\ 0 & \widetilde{\mathbf{S}}_E^{11} \end{bmatrix}. \tag{36}$$

In general, $\widetilde{\mathbf{S}}_E^{11}$ is a positive definite matrix for a positive definite tensor v, and becomes diagonal when v is a scalar field.

The matrix $\widetilde{\mathbf{A}}_E^{22}$ can be *any symmetric and positive definite matrix* with eigenvalues close to the maximum eigenvalue of $\widetilde{\mathbf{A}}_E^{11}$, thus providing us with *a family* of numerical methods with equivalent approximation properties. In practice, a reasonable choice for $\widetilde{\mathbf{A}}_E^{22}$ is the scalar matrix,

$$\widetilde{\mathbf{A}}_E^{22} = \lambda_{max}(v) |E| \mathbf{I}_{\mathcal{D}-6}, \tag{37}$$

where $\lambda_{max}(v)$ is the maximum eigenvalue of v.

We conclude this subsection with a lemma that proves the invertibility of the matrix $\mathbf{T}_E$. This result establishes the well-posedness of the previous construction because it guarantees that the vectors $\{T_j\}_j$ with $j = 1, \ldots, \mathcal{D}$, i.e. the columns of the matrix $\mathbf{T}_E$, are linearly independent and form a basis for X_E^h.

Lemma 1. *The matrix* $\mathbf{T}_E \in \mathbb{R}^{\mathcal{D}\times\mathcal{D}}$ *is non singular.*

Proof. The proof is by contradiction. Assume that matrix $\mathbf{T}_E$ is singular. Then, there must exist a vector $V \neq 0$, such that $\mathbf{T}_E V = 0$. By multiplying this equation by $\mathbf{R}_E^T$ and using (31)–(33), we obtain

$$0 = \mathbf{R}_E^T\mathbf{T}_E V = [\mathbf{R}_E^T\mathbf{T}_{1..6}, \mathbf{R}_E^T\mathbf{T}_{7..\mathcal{D}}]V = \widetilde{\mathbf{A}}_E^{11}[V_1, V_2, .., V_6]^T \;\Rightarrow\; \widetilde{\mathbf{S}}_E^{11}[V_4, V_5, V_6] = 0. \tag{38}$$

Since $\widetilde{\mathbf{S}}_E^{11}$ is positive definite, the above identity gives $V_4 = V_5 = V_6 = 0$. Due to the definitions of T_1, T_2, T_3 and the orthogonality relations in (34) and (35), the columns $\{T_j\}_j$ with $j = 1, 2, 3$ and $j = 7, 8, \ldots, \mathcal{D}$ are linearly independent. Therefore, a zero linear combination of these column vectors is possible only when all the coefficients of the linear combination are zero, which implies that $V = 0$. This fact contradicts the initial fact that $V \neq 0$ and, hence, proves the assertion of the lemma. □

3.2.4. Inexpensive construction of the stiffness matrix $\mathbf{A}_E$

The calculation of the matrix $\mathbf{A}_E$ involves the inversion of the transformation matrix $\mathbf{T}_E$ and three full matrix–matrix products, which all require $\mathcal{O}(\mathcal{D}^3)$ floating-point operations. To get an insight about these costs, note that, for instance, $\mathcal{D} = 12$ for a quadrilateral element, thus producing a 12×12 matrix $\mathbf{T}_E$. However, the complexity of the procedure described in Section 3.2.3 must be compared with the complexity of the iterative solvers for the saddle point problem (14). Thus, the cost of the matrix construction is expected to be small (but not negligible) with respect to the global cost of the method.

In this subsection, we present a slight modification of the previously described procedure, that yields a more efficient method for the calculation of $\mathbf{A}_E$. Property (32) implies that

$$\mathbf{R}_{4..6}^T\mathbf{T}_{4..6} = \widetilde{\mathbf{S}}_E^{11}.$$

Thus, the general form of the matrix $\mathbf{A}_E$ that satisfies (27) is given by

$$\mathbf{A}_E = \mathbf{R}_{4..6}(\widetilde{\mathbf{S}}_E^{11})^{-1}\mathbf{R}_{4..6}^T + \mathbf{P}\mathbf{U}_E\mathbf{P}, \tag{39}$$

where $\mathbf{U}_E$ is an arbitrary symmetric positive definite matrix and $\mathbf{P}$ is the orthogonal projector,

$$\mathbf{P} = \mathbf{I}_{\mathcal{D}} - \mathbf{T}_{1..6}(\mathbf{T}_{1..6}^T\mathbf{T}_{1..6})^{-1}\mathbf{T}_{1..6}^T. \tag{40}$$

This new matrix $\mathbf{A}_E$ belongs to the same family of matrices given by (18) and (19). Nonetheless, equations (39) and (40) only require the inversion of the 3×3 matrix $\widetilde{\mathbf{S}}_E^{11}$ and the 6×6 matrix $\mathbf{T}_{1-6}^T\mathbf{T}_{1-6}$, independently of the number of polygonal edges and thus of the value of $\mathcal{D}$. Moreover, for a scalar coefficient v, the matrix $\widetilde{\mathbf{S}}_E^{11}$ has a very simple form with a negligible inversion cost: $\widetilde{\mathbf{S}}_E^{11} = 2v|E|\mathbf{I}_3$.

If we choose $\mathbf{U}_E$ to be a scalar matrix, e.g. $\mathbf{U}_E = 2v|E|\mathbf{I}_6$, formula (39) is simplified to

$$\mathbf{A}_E = \frac{1}{2v|E|}\mathbf{R}_{4..6}\mathbf{R}_{4..6}^T + 2v|E|\mathbf{P}. \tag{41}$$

The structure of the 6×6 matrix $\mathbf{T}_{1..6}^T\mathbf{T}_{1..6}$ can be further simplified on *Cartesian grids* by shifting the coordinate system to the center of mass of E. In this case, the vectors T_1 and T_3 (corresponding to ϕ_1 and ϕ_3, respectively) are orthogonal to the remaining vectors and, after a suitable rearrangement of columns and rows, $\mathbf{T}_{1..6}^T\mathbf{T}_{1..6}$ becomes a block-diagonal matrix, thus permitting a further reduction of the inversion cost.

Remark 2. The existence of the basis functions $\{\phi_i\}$ for each element E that produce a given matrix $\mathbf{A}_E$ can be investigated using the technique described in [14] for the diffusion problem.

3.3. Discretization of $\mathcal{B}(p, \mathbf{v})$

We reduce the discretization of the global bilinear forms $\mathcal{B}(p, \mathbf{v})$ to the discretization of the elemental bilinear form $\mathcal{B}_E(p_E, \mathbf{v}_E)$ through the assembly decomposition:

$$\mathcal{B}(p, \mathbf{v}) := \sum_{E\in\Omega^h} \mathcal{B}_E(p_E, \mathbf{v}_E).$$

Since the pressure p_E is approximated by a constant function on each polygonal element E, using the Gauss divergence theorem yields:

$$\mathcal{B}_E(p_E, \mathbf{v}_E) \equiv \int_E p_E \mathrm{div}(\mathbf{v}_E)\, d\mathbf{x} = p_E \int_E \mathrm{div}(\mathbf{v}_E)\, d\mathbf{x} = p_E \int_{\partial E} \mathbf{v}_E \cdot \mathbf{n}_E\, ds = p_E \sum_{e_i\in\partial E} \int_{e_i} \mathbf{v}_E \cdot \mathbf{n}_E\, ds = p_E \sum_{e_i\in\partial E} |e_i| V_i^e.$$

The arguments of the final summation are the fluxes through the edges of E, which belong to the set of degrees of freedom introduced in Section 3.

3.4. Discretization of $\mathcal{L}(\mathbf{v})$

We rewrite $\mathcal{L}(\mathbf{v})$ as follows:

$$\mathcal{L}(\mathbf{v}) = \sum_{E\in\Omega^h} \int_E \mathbf{F}\cdot\mathbf{v}\,d\mathbf{x} + \sum_{e\in\Gamma_N} \int_e \mathbf{h}\cdot\mathbf{v}\,ds. \tag{42}$$

In Eq. (42), we approximate the volume integrals by assuming that $\mathbf{F}(\mathbf{x})$ is constant over each element E and the edge integrals by assuming that $\mathbf{h}(\mathbf{x})$ is constant on each boundary edge $e \in \Gamma_N$. In the former case, we define a quadrature rule by using the vertices of E as quadrature points and a suitable set of positive weights $\{\omega_i\}_i$. For the weights ω_i, we use the same coefficients of the formula that provides the center of gravity of E as the linear combination of the position vectors of the vertices of the element. By construction, this quadrature rule is exact for linear functions. Applying this quadrature rule to the first integral in the right-hand side of (42) yields

$$\int_E \mathbf{F}\cdot\mathbf{v}_E\,d\mathbf{x} \approx \sum_{i=1}^{\mathcal{N}(E)} \omega_i \mathbf{F}(\mathbf{x}_E)\cdot\mathbf{v}_E(\mathbf{a}_i) = \sum_{i=1}^{\mathcal{N}(E)} \omega_i \left(V_i^x, V_i^y\right)^T \cdot \mathbf{F}(\mathbf{x}_E), \tag{43}$$

where $\mathbf{x}_E$ denotes the center of mass of E.

For the second integral in (42), we proceed as follows. Let e_i be the i-th edge of the polygonal element E and $\mathbf{x}_i$ be its midpoint. By using the notation of Fig. 1, assumptions **A1**–**A2** and integration formula (24), we obtain:

$$\begin{aligned}\int_{e_i} \mathbf{h}\cdot\mathbf{v}_E\,ds &\approx \mathbf{h}(\mathbf{x}_i)\cdot\int_{e_i}\mathbf{v}_E\,ds = (\mathbf{h}(\mathbf{x}_i)\cdot\mathbf{n}_i)\int_{e_i}\mathbf{v}_E\cdot\mathbf{n}_i\,ds + (\mathbf{h}(\mathbf{x}_i)\cdot\mathbf{t}_i)\int_{e_i}\mathbf{v}_E\cdot\mathbf{t}_i\,ds \\ &= (\mathbf{h}(\mathbf{x}_i)\cdot\mathbf{n}_i)|e_i|V_i^e + (\mathbf{h}(\mathbf{x}_i)\cdot\mathbf{t}_i)\frac{|e_i|}{2}\left(V_i^x + V_{i+1}^x,\, V_i^y + V_{i+1}^y\right)^T\cdot\mathbf{t}_i.\end{aligned} \tag{44}$$

3.5. Boundary conditions

In the variational formulation of Section 2, the Dirichlet boundary conditions manifest themselves through the admissible class $X_{\mathbf{g}}$, c.f. (4), while the Neumann boundary conditions only affect the linear functional $\mathcal{L}(\mathbf{v})$, c.f. (5). In the corresponding mimetic formulation, the Dirichlet boundary conditions appear through the definition of the class $X_{\mathbf{g}}^h$ and the space X_0^h.

In practical implementations, we directly prescribe the values of the degrees of freedom of the vertices and edges on the boundary Γ_D. Thus, for each boundary vertex $\mathbf{a}_i \in \Gamma_D$ we set

$$\left(U_i^x, U_i^y\right)^T := \mathbf{g}(\mathbf{a}_i), \tag{45}$$

and for each boundary edge $e_i \in \Gamma_D$ we set

$$U_i^e := \frac{1}{|e_i|}\int_{e_i}\mathbf{g}(s)\cdot\mathbf{n}_E\,ds. \tag{46}$$

Let us denote by U_0 and V_0 the subsets of U and V, respectively, that does not contain the degrees of freedom specified by the Dirichlet boundary conditions (45) and (46). Substituting (45) and (46) into (13) and eliminating the equations corresponding to the Dirichlet degrees of freedom, we obtain the linear system given in (14) for U_0 and P.

4. Stability analysis

In this section, we show that the above presented MFD discretization is stable. This property is important for demonstrating the solvability of the linear system and the convergence of the numerical method. The stability analysis for saddle point problems [12] requires to prove two inequalities. The first inequality is the coercivity of the bilinear form $\mathcal{A}$ with respect to a natural norm in X^h (see Theorem 1). The second inequality is the *inf-sup* condition (see Theorem 2).

4.1. Coercivity of bilinear form $\mathcal{A}$

The main result of this section is the coercivity of the bilinear form

$$\mathcal{A}(\mathbf{v},\mathbf{v}) = V^T A V$$

in the approximation space X_0 with respect to the natural norm defined by Eq. (49).

4.1.1. Natural norm in X_0^h

Since the shape functions $\phi_7,\ldots,\phi_{\mathcal{D}(E)}$ are not known inside E, we cannot use the H^1-norm for the space X_0^h. Thus, our first goal is to define an analog of the H^1-norm that uses only known information about the space X_0^h. Due to assumptions **(A1)** and **(A2)**, for any $V_E \in X_E^h$, the corresponding vector function $\mathbf{v}_E \in \mathcal{V}_E$ is completely determined only on the boundary edges of

E. Hence, we define a norm that depends on the derivatives of the functions along the edges of E and transform appropriately under change of coordinates and coordinate scaling. Let us define the following seminorm on X_E^h:

$$|||V_E|||_E^2 := \sum_{i=1}^{\mathcal{N}(E)} |e_i| \int_{e_i} \left(\frac{d}{ds} \mathbf{v}_E(s) \right)^2 ds \quad \forall V_E \in X_E^h, \tag{47}$$

where $\frac{d}{ds}$ is the tangential derivative along e_i. Recall that the basis functions ϕ_1, ϕ_2, ϕ_3 represent the rigid motions of E and correspond to the basis vectors $T_1, T_2, T_3 \in X_E^h$. The natural local seminorm that vanishes on rigid body motions is given by

$$|||V_E|||_{\star,E} := \min_{\underline{c} \in \mathbb{R}^3} |||V_E + \mathbf{T}_{1..3} \underline{c}|||_E \quad \forall V_E \in X_E^h. \tag{48}$$

In the above definition, we can neglect the contributions from ϕ_1 and ϕ_3, because the differentiation in (47) ignores constant functions. Eventually, from (47), (48) we define the "broken" seminorm on the space X^h:

$$|||V|||_*^2 := \sum_{E \in \Omega^h} |||V_E|||_{*,E}^2. \tag{49}$$

This seminorm is a norm on the space X_0^h, since X_0^h does not contain non-trivial rigid motions as shown in Lemma 3. The goal of the next subsections is to prove the coercivity of the bilinear form $\mathcal{A}$ with respect to the norm $|||\cdot|||_*$ in X_0^h.

We will use $\|\cdot\|$ to denote the standard Euclidean norm on $\mathbb{R}^m$. Whenever m is different from $\mathcal{D}$, we use the lower-case letters $\underline{v}, \underline{u}$ and $\underline{w}$ to indicate vectors in $\mathbb{R}^m$ and introduce the following seminorm (which ignores the first three components of a vector):

$$\|\underline{v}\|_\star^2 := \sum_{i=4}^{m} v_i^2 \quad \forall \underline{v} \in \mathbb{R}^m, \ m > 3.$$

4.1.2. Mesh regularity assumptions

A few quite general mesh assumptions from [11] are required for the following analysis. We assume that there exists a compatible decomposition S_h of the polygonal mesh Ω_h into triangles. Moreover, there exist two mesh independent numbers $N_* \in \mathbb{N}$ and $\rho_* > 0$, such that:

- every polygon $E \in \Omega_h$ admits a decomposition $S_h|_E$ made of less than N_* triangles;
- for each triangle $T \in S_h$, the ratio of the radius of the inscribed disk to the diameter of T is bounded from below by ρ_*.

We do not need to build the decomposition S_h explicitly but only know that we can do it, i.e. this decomposition does exist. The consequences of these mesh assumptions are:

- the number of edges $\mathcal{N}(E)$ of each polygon E is uniformly bounded;
- there exists a constant σ_* that depends only on N_* and ρ_*, such that it holds:

$$|e_i| \geqslant \sigma_* \mathrm{diam}(E) \quad \text{and} \quad |E| \geqslant \sigma_* \mathrm{diam}(E)^2$$

for every edge e_i of E.

4.1.3. Main result: coercivity of $\mathcal{A}(\mathbf{v}, \mathbf{v})$

Hereafter, C, C_1 and C_2 are *positive* constants that are possibly different at each occurrence. These constants are independent of the mesh but may depend on the tensor v and the shape regularity parameters N_*, ρ_* and σ_*, introduced in Section 4.1.2.

Lemma 2. *The symmetric 3×3 matrix $\widetilde{\mathbf{S}}_E^{11}$, introduced in (36), satisfies*

$$C_1 |E| \, \|\underline{v}\|^2 \leqslant \underline{v}^T \, \widetilde{\mathbf{S}}_E^{11} \, \underline{v} \leqslant C_2 |E| \, \|\underline{v}\|^2 \quad \forall \underline{v} \in \mathbb{R}^3. \tag{50}$$

Proof. Note that $D(\phi_4), D(\phi_5), D(\phi_6)$ are constant tensors. With a scaling argument, we get

$$(\widetilde{\mathbf{S}}_E^{11})_{(i-3)(j-3)} = 2 \int_E v D(\phi_i) : D(\phi_j) d\mathbf{x} = 2|E|(v D(\phi_i) : D(\phi_j)) \quad i,j = 4,5,6. \tag{51}$$

The result follows from the fact that v is a positive definite tensor. □

As a consequence of the scaling choice (37) we also have

$$C_1 |E| \, \|\underline{v}\|^2 \leqslant \underline{v}^T \, \widetilde{\mathbf{A}}_E^{22} \, \underline{v} \leqslant C_2 |E| \, \|\underline{v}\|^2 \quad \forall \underline{v} \in \mathbb{R}^{\mathcal{D}-6}. \tag{52}$$

By definition, first using (18), (19) and then (36) we infer that

$$V_E^T \mathbf{A}_E V_E = \underline{w}^T \widetilde{\mathbf{A}}_E \underline{w} = \underline{u}^T \widetilde{\mathbf{A}}_E^{11} \underline{u} + \underline{v}^T \widetilde{\mathbf{A}}_E^{22} \underline{v} = (u_4, u_5, u_6) \widetilde{\mathbf{S}}_E^{11} (u_4, u_5, u_6)^T + \underline{v}^T \widetilde{\mathbf{A}}_E^{22} \underline{v}.$$

From this equality, using Lemma 2 and (52 it immediately follows that

$$C_1 |E| (\|\underline{u}\|_\star^2 + \|\underline{v}\|^2) \leqslant V_E^T \mathbf{A}_E V_E \leqslant C_2 |E| (\|\underline{u}\|_\star^2 + \|\underline{v}\|^2) \tag{53}$$

for all $V_E \in X_E^h$, $\underline{u} \in \mathbb{R}^6$ and $\underline{v} \in \mathbb{R}^{\mathcal{D}-6}$, such that

$$V_E = \mathbf{T} [\underline{u}^T, \underline{v}^T]^T = \mathbf{T}_{1..6} \underline{u} + \mathbf{T}_{7..\mathcal{D}} \underline{v}. \tag{54}$$

We can now present the following result.

Proposition 1. *There exists a positive constant α_E, dependent only on the tensor ν and the shape regularity parameters N_*, ρ_* and σ_* introduced in Section 4.1.2, such that*

$$\mathcal{A}_E(\mathbf{v}_E, \mathbf{v}_E) = V_E^T \mathbf{A}_E V_E \geqslant \alpha_E |||V_E|||_{*,E}^2 \quad \forall V_E \in X_E^h.$$

Proof. Let $V_E \in X_E^h \equiv \mathbb{R}^{\mathcal{D}}$. Since the matrix $\mathbf{T}$ is invertible, for each V_E, there exist two unique vectors $\underline{u} \in \mathbb{R}^6$ and $\underline{v} \in \mathbb{R}^{\mathcal{D}-6}$, such that

$$V_E = \mathbf{T} [\underline{u}^T, \underline{v}^T]^T = \mathbf{T}_{1.6} \underline{u} + \mathbf{T}_{7.\mathcal{D}} \underline{v}$$

Due to the $\mathcal{A}_E$-orthogonality condition (33) we have the following decomposition

$$V_E^T \mathbf{A}_E V_E = \underline{u}^T (\mathbf{T}_{1..6}^T \mathbf{A}_E \mathbf{T}_{1..6}) \underline{u} + \underline{v}^T (\mathbf{T}_{7..\mathcal{D}}^T \mathbf{A}_E \mathbf{T}_{1..\mathcal{D}}) \underline{v} = \underline{u}^T \widetilde{\mathbf{A}}_E^{11} \underline{u} + \underline{v}^T \widetilde{\mathbf{A}}_E^{22} \underline{v}. \tag{55}$$

The definition of matrix $\widetilde{\mathbf{A}}_E^{11}$ and scaling assumption (35) imply that

$$\underline{u}^T \widetilde{\mathbf{A}}_E^{11} \underline{u} \geqslant C|E| \|\underline{u}\|_\star^2 \quad \text{and} \quad \underline{v}^T \widetilde{\mathbf{A}}_E^{22} \underline{v} \geqslant C|E| \|\underline{v}\|^2 \tag{56}$$

Since all the derivatives of $\phi_j (j = 4, 5, 6)$ are bounded by 1, and $|e_i|^2 \leqslant C|E|$, we get

$$|||\mathbf{T}_{1..6} \underline{u}|||_{*,E}^2 \leqslant C \sum_{j=4}^{6} u_j^2 \sum_{i=1}^{\mathcal{D}} |e_i|^2 \leqslant C|E| \|\underline{u}\|_\star^2. \tag{57}$$

We now observe that, for any $W_E \in X_E^h$, the definition of the degrees of freedom in Section 3.1 implies that

$$\|\mathbf{w}_E\|_{L^\infty(\partial E)}^2 \leqslant C \|W_E\|^2 \quad \forall W_E \in X_E^h, \tag{58}$$

where $\mathbf{w}_E$ is the associated function to W_E. Since the restriction of $\mathbf{w}_E$ to the boundary is a piecewise polynomial function, an edge-by-edge standard inverse inequality gives

$$|||W_E|||_{*,E}^2 \leqslant |||W_E|||_E^2 = \sum_{i=1}^{\mathcal{N}(E)} |e_i| \int_{e_i} \left(\frac{d}{ds} \mathbf{w}_E(s) \right)^2 ds \leqslant C \|\mathbf{w}_E\|_{L^\infty(\partial E)}^2. \tag{59}$$

Using (59), (58) and recalling the scaling assumption (35) yields

$$|||\mathbf{T}_{7..\mathcal{D}} \underline{v}|||_{*,E}^2 \leqslant C \|\mathbf{T}_{7..\mathcal{D}} \underline{v}\|^2 = C|E| \|\underline{v}\|^2. \tag{60}$$

Thus, combining (55)–(57) with (60) and using the triangle inequality, we obtain the desired estimate:

$$V_E^T \mathbf{A}_E V_E \geqslant C(|||\mathbf{T}_{1..6} \underline{u}|||_{*,E}^2 + |||\mathbf{T}_{7..\mathcal{D}} \underline{v}|||_{*,E}^2) \geqslant \frac{C}{2} |||V_E|||_{*,E}^2 \quad \forall V_E \in X_E^h.$$

Taking $\alpha_E = C/2$, completes the proof. □

The bilinear form $\mathcal{A}_E(\mathbf{v}_E, \mathbf{v}_E)$ is also h-uniformly continuous with respect to the same norm $|||\cdot|||_\star$. This result is proven in Proposition 2 in the Appendix.

Lemma 3. *The seminorm $|||\cdot|||_*$, defined by (49), is a norm on the space X_0^h if Ω^h is a connected partition of the domain Ω.*

Proof. Clearly, $|||\cdot|||_*$ is a seminorm on X_0^h. Thus, it only remains to show that for any $V \in X_0^h$, $|||V|||_* = 0$ implies that $V_E = 0$. Let us first observe that $V_E = 0$ on the whole element E when V_E is a rigid motion on the element E and $V_E = 0$ on one of the edges $e \subset \partial E$. In such a case, it also follows that $V_E = 0$ on all the other edges of the element E.

Now, let us consider a vector $V \in X_0^h$ such that $|||V|||_* = 0$. From definition (49) it follows that $|||V_E|||_{*,E} = 0$ for all the elements $E \in \Omega^h$. In view of (48) and (47), V represents the rigid body motions on each element E, and $V_E = 0$ in each E having an edge on the Dirichlet boundary Γ_D, which is assumed non-empty. Since V is continuous across mesh elements and Ω^h is a

connected partition of the domain Ω, we can propagate the above argument everywhere starting from the edges of the Dirichlet boundary Γ_D. □

Theorem 1. *Let Ω^h be a connected partition. Then, there exists a positive constant α, dependent only on α_E, such that*

$$V^T\mathbf{A}V \geqslant \alpha |||V|||_*^2 \quad \forall V \in X^h. \tag{61}$$

Proof. Let E be an element of the partition Ω^h and α_E be the constant introduced in Proposition 1. We define $\alpha = \min_{E\in\Omega^h}\alpha_E$. Then, using Proposition 1 and recalling (49), we infer that

$$V^T\mathbf{A}V = \sum_{E\in\Omega^h} V_E^T\mathbf{A}_E V_E \geqslant \sum_{E\in\Omega^h} \alpha_E |||V_E|||_{*,E}^2 \geqslant \alpha \sum_{E\in\Omega^h} |||V_E|||_{*,E}^2 = \alpha |||V|||_*^2. \tag{62}$$

This proves the theorem. □

Remark 3. It may be interesting to observe that Proposition 1 allows also to prove a coercivity result in the L^∞ norm; the proof can be found in [7]. If meas $(\Gamma_D) > 0$ then

$$\mathcal{A}(\mathbf{v},\mathbf{v}) = V^T\mathbf{A}V \geqslant \frac{C}{\ln(2+1/h)}\|V\|_\infty^2 \quad \forall V \in X^h, \tag{63}$$

where C is independent of h, $\|\cdot\|_\infty$ indicates the maximum norm on vectors, and V is the vector representation of $\mathbf{v}$.

4.2. Inf-sup condition

In the following theorem we briefly sketch the proof of the *inf-sup condition* (the second condition required for the analysis of the stability).

Theorem 2. *There exists a positive constant β (independent of h), such that for all $S \in Q^h$ (and the associated piecewise constant function s) there exists $V \in X_0^h$ (and the associated piecewise regular function $\mathbf{v}$), such that*

$$\mathcal{B}(s,\mathbf{v}) \geqslant \beta\left(\sum_{E\in\Omega_h} |E|\,|s_E|^2\right)^{\frac{1}{2}} \quad \text{and} \quad |||V|||_* \leqslant 1. \tag{64}$$

Proof. Due to the well known inf-sup condition [12] for the continuous problem, for any $s \in L_0^2(\Omega)$ there exists $\tilde{\mathbf{v}} \in X_0$ and a positive constant β' (independent of s), such that

$$\mathcal{B}(s,\tilde{\mathbf{v}}) \geqslant \beta'\|s\|_{L^2(\Omega)} = \beta'\left(\sum_{E\in\Omega_h} |E|\,|s_E|^2\right)^{\frac{1}{2}} \quad \text{and} \quad \|\tilde{\mathbf{v}}\|_{H^1(\Omega)} \leqslant 1. \tag{65}$$

Let $\tilde{\mathbf{v}}_c$ be the piecewise linear Clément interpolation [19] of $\tilde{\mathbf{v}}$ on the sub-mesh S_h. Such an interpolation satisfies the bound

$$\|\tilde{\mathbf{v}}_c\|_{H^1(\Omega)} \leqslant C\|\tilde{\mathbf{v}}\|_{H^1(\Omega)} \leqslant C. \tag{66}$$

We define $V \in X_0^h$ (and the related $\mathbf{v}$) on each element E by

$$\begin{aligned} &(V_i^x, V_i^y) = \tilde{\mathbf{v}}_c(\mathbf{a}_i) \quad i = 1,\dots,\mathcal{N}(E) \\ &V_i^e = \frac{1}{|e_i|}\int_{e_i} \tilde{\mathbf{v}}(s)\cdot\mathbf{n}_e\,ds \quad i = 1,\dots,\mathcal{N}(E). \end{aligned} \tag{67}$$

Due to $(67)_2$ and the definition of $\mathcal{B}$ it is easy to check that

$$\mathcal{B}(s,\mathbf{v}) = \sum_{E\in\Omega_h} s_E \sum_{e_i\in\partial E}\int_{e_i}\tilde{\mathbf{v}}\cdot\mathbf{n}_e\,ds = \sum_{E\in\Omega_h} s_E\int_E \operatorname{div}(\tilde{\mathbf{v}})\,dx = \mathcal{B}(s,\tilde{\mathbf{v}})$$

which together with the first property in (65) immediately implies the first part of (64). The second bound in (64) follows with a scaling argument and recalling (66). □

5. Numerical experiments

To measure the quality of the numerical solution, we use the two mesh-dependent L^2 norms

$$|||V|||_X = \left[\sum_{E\in\Omega^h} |E| V_E^T V_E\right]^{1/2} \quad \text{and} \quad |||P|||_Q = \left[\sum_{E\in\Omega^h} |E| P_E^2\right]^{1/2},$$

and the one H^1-type norm

$$|||V|||^2 := \sum_{E\in\Omega^h} |||V_E|||_E^2. \tag{68}$$

Note that we use the stronger norm (68) instead of norm (49) that appears in Theorem 1 because the first norm is simpler to compute and, due to the boundary conditions, is essentially equivalent to the second one.

To solve the saddle point problem (14), we use the iterative solvers with block-diagonal preconditioners of the form

$$\begin{bmatrix} \mathbf{H}_0 & 0 \\ 0 & \mathbf{M} \end{bmatrix},$$

where $\mathbf{H}_0$ is a preconditioner for the matrix $\mathbf{A}_0$ and $\mathbf{M}_0$ is the diagonal mass matrix with areas $|E|$ on the diagonal. To achieve a mesh independent convergence of the iterative process, the matrix $\mathbf{H}_0$ must be spectrally equivalent to $\mathbf{A}_0$. We have verified this for small mesh resolutions and $\mathbf{H}_0 = \mathbf{A}_0^{-1}$. However, we have not achieved spectral equivalence with either the W-cycle of the algebraic multigrid [34] or the second-order accurate incomplete LU factorization [28].

5.1. Random quadrilateral meshes

Let Ω be a unit square and $v = 1/2$. We impose the Dirichlet boundary conditions on three sides of the unit square and the Neumann boundary condition of the remaining side. These conditions are chosen such that the exact solution is

$$\mathbf{u}(x,y) = \begin{bmatrix} y^3 + x \\ x^3 - y \end{bmatrix}, \quad p(x,y) = 3xy - .75. \tag{69}$$

We consider a sequence of randomly perturbed quadrilateral meshes (see Fig. 2). A randomly perturbed mesh is built from a square mesh with mesh size $h = 1/n$ by relocating each interior mesh node $\mathbf{a}$ to a random position inside a square box. The box is centered at $\mathbf{a}$, its sides are aligned with the coordinate axis, and its size is $h/2$.

The convergence analysis on the sequence of randomly perturbed meshes is the most challenging test for any discretization method. Fig. 3 shows the second-order convergence rate for the discrete L^2 norm of the velocity error and the first-order for the discrete L^2 norm of the pressure error and the discrete H^1 norm (68) of the velocity error.

5.2. Polygonal meshes

Let Ω be, again, a unit square and $v = 1/2$. We consider the Dirichlet boundary value problem with the exact solution

$$\mathbf{u}(x,y) = e^{x+y}\begin{bmatrix} 1 \\ -1 \end{bmatrix}, \quad p(x,y) = 0.$$

Contrary to (69) this solution results in a non-zero right-hand side.

We study convergence of the method on a sequence of polygonal meshes. A polygonal mesh (see Fig. 2) is built in two steps. First, we generate the Voronoi tessellation for the set of points $(x_{i,j}, y_{i,j})$ given by

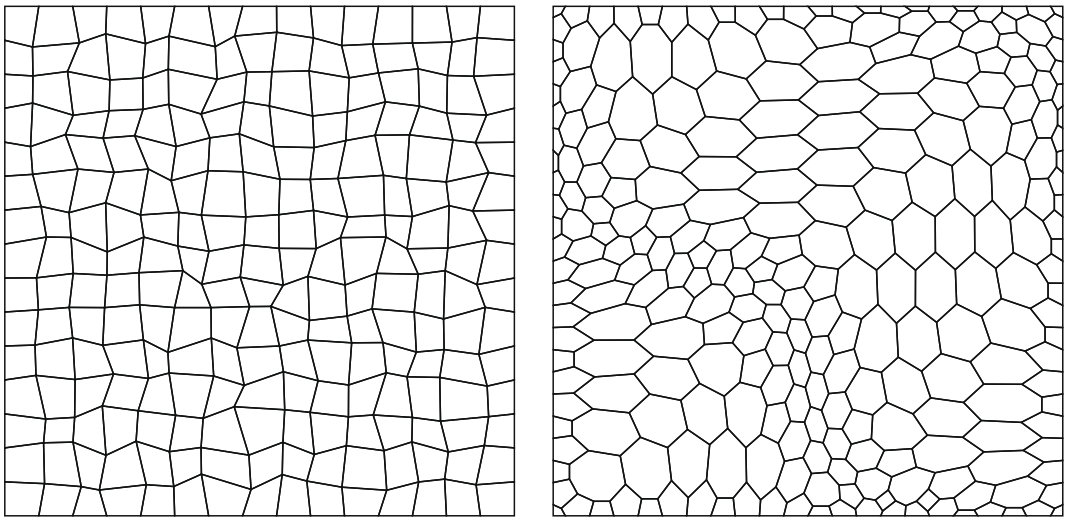

Fig. 2. A sample 15×15 quadrilateral mesh with randomly perturbed vertices and a sample polygonal mesh.

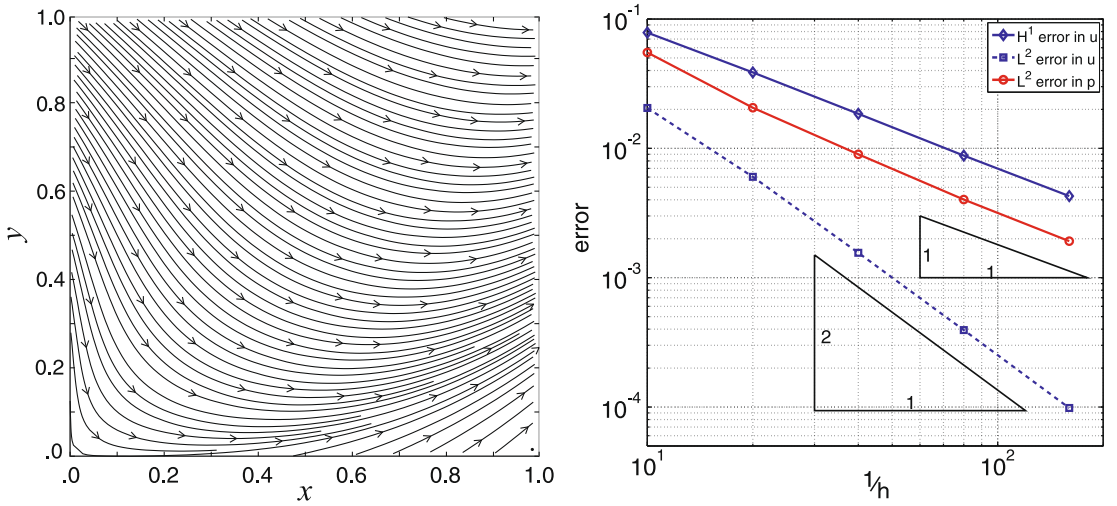

Fig. 3. Left picture shows the streamlines for the discrete solution on the finest mesh. Right picture shows graphs of the mesh-dependent L^2 and H^1 norms of the errors. The velocity graphs are marked by diamonds and squares (blue lines) and the pressure graph is marked by circles (red line). (For interpretation of the references in color in this figure legend, the reader is referred to the web version of this article.)

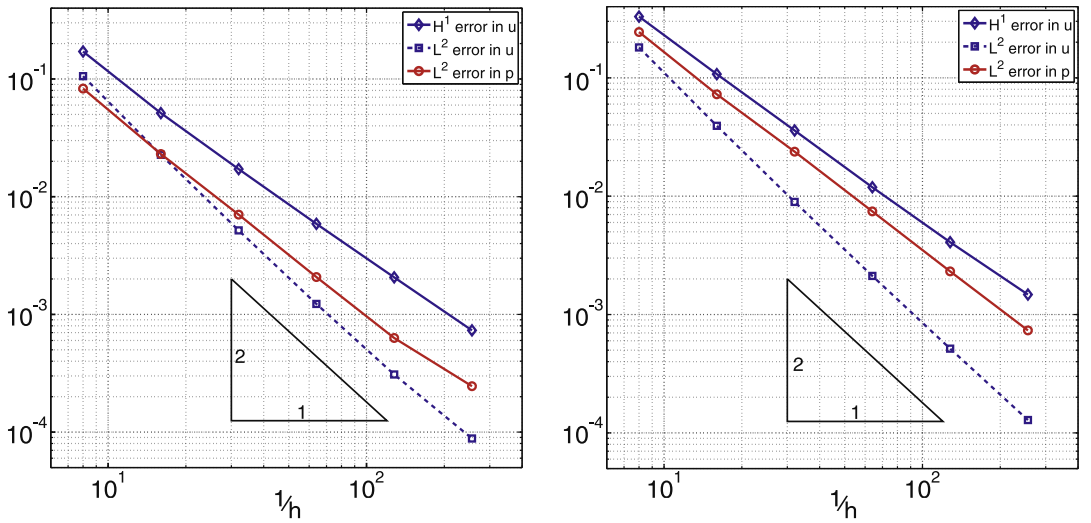

Fig. 4. Graphs (left is for ν that is a scalar and right is for ν that is a tensor) of the mesh-dependent L^2 and H^1 norms of the errors. The velocity graphs are marked by diamonds and squares (blue lines) and the pressure graphs are marked by circles (red lines). The average slopes of the error for p are 1.70 and 1.67, respectively. (For interpretation of the references in color in this figure legend, the reader is referred to the web version of this article.)

$$x_{i,j} = \xi_i + 0.1\,\sin(2\pi\xi_i)\,\sin(2\pi\eta_j), \quad i = 0,\ldots,n,$$
$$y_{i,j} = \eta_j + 0.1\,\sin(2\pi\xi_i)\,\sin(2\pi\eta_j), \quad j = 0,\ldots,n,$$

where $\xi_i = ih, \eta_j = jh$ and $h = 1/n$. Second, we move each interior mesh node **a** to the center of mass of a triangle formed by the centers of three Voronoi cells sharing **a**.

As shown in Fig. 4, we observe the second-order convergence rate for the discrete L^2 norm of the velocity error. Superconvergence is observed for the discrete H^1 norm of the velocity error (of order 1.6) and the discrete L^2 norm of the pressure error (of order 1.7). This probably reflects the fact that the sequence of polygonal meshes has been built using a smooth map.

5.3. Polygonal meshes and tensor coefficients

Let us consider the previous example but replace the constant viscosity ν by a symmetric fourth-order tensor ν satisfying (2). Let $\boldsymbol{\varepsilon} = D(\mathbf{u})$. Using the reduced Voigt notation, the symmetric tensor is defined by six independent components:

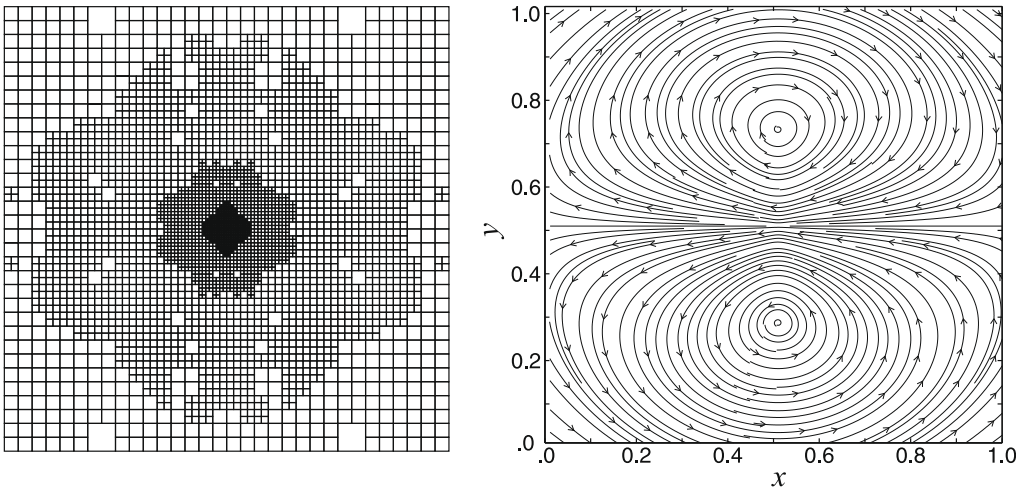

Fig. 5. Left picture shows the locally refined mesh after three adaptive iterations. Right picture shows streamlines of the discrete solution on the most refined mesh.

Table 1
Convergence on a sequence of locally refined meshes.

$\mathcal{N}(\Omega^h)$	$\|\|\|U^{ex}-U\|\|\|_X$	$\|\|\|U^{ex}-U\|\|\|_*$	$\|\|\|P^{ex}-P\|\|\|_Q$	$\sqrt{\int \|P^{ex}-P\|^2 x\,dV}$
256	4.47e−2	6.04e−1	2.47e−1	4.80e−2
472	2.56e−2	7.04e−1	2.48e−1	3.53e−2
928	1.46e−2	8.06e−1	2.47e−1	2.53e−2
1924	8.06e−3	9.01e−1	2.47e−1	1.74e−2
3868	4.45e−3	1.02e−0	2.47e−1	1.24e−2

$$\begin{bmatrix}\sigma_{xx}\\ \sigma_{yy}\\ \sigma_{xy}\end{bmatrix} = 2\begin{bmatrix}\nu_{11} & \nu_{12} & \nu_{13}\\ \nu_{12} & \nu_{22} & \nu_{23}\\ \nu_{13} & \nu_{33} & \nu_{33}\end{bmatrix}\begin{bmatrix}\varepsilon_{xx}\\ \varepsilon_{yy}\\ \varepsilon_{xy}\end{bmatrix} - \begin{bmatrix}p\\ p\\ 0\end{bmatrix}.$$

This problem is an intermediate step towards the displacement formulation of a linear elasticity problem. Therefore, we set $\nu_{11}=\nu_{22}=\lambda+2\mu$, $\nu_{12}=\lambda$ and $\nu_{33}=4\mu$, all other coefficients are then equal to zero. The anisotropic tensor is obtained by setting $\lambda=5$ and $\mu=1/2$.

The right picture in Fig. 4 shows the second-order convergence rate for the discrete H^1 norm of the velocity error. Again, slight superconvergence is observed for the other two errors. Comparing the two pictures in Fig. 4, we see that the effect of the tensor anisotropy is mild. All errors are roughly twice bigger than that for the scalar coefficient ν.

5.4. Locally refined meshes

Let Ω be again the unit square centered at the origin and $\nu=1$. We consider the Dirichlet boundary value problem with the point force $\mathbf{F}=(-\delta(0,0),0)^T$. The exact solution is

$$\mathbf{u}(x,y)=\frac{1}{8\pi}\begin{bmatrix}1+\log(x^2+y^2)+\frac{2y^2}{x^2+y^2}\\ \frac{-2xy}{x^2+y^2}\end{bmatrix},\quad p(x,y)=\frac{-4x}{x^2+y^2}. \tag{70}$$

We study convergence of the method on a sequence of locally refined meshes. The sequence starts with the uniform square 16×16 mesh. The singular point force is approximated by a piecewise constant function with unit integral. On each mesh in the sequence, this function equals to zero almost everywhere except in four square cells in the middle of the domain. The mesh refinement is based on a simple error indicator – sum of pressure jumps across mesh edges. The error threshold for mesh refinement is the average value of this indicator.

Fig. 5 indicates strong refinement towards the domain center where the solution is singular. Since p is not in $L^2(\Omega)$, we cannot expect convergence for the discrete L^2 norm of the pressure error, see Table 1. Clearly, this is not a failure of the method but an unavoidable consequence of the problem. For the same reason, the discrete H^1 norm of the velocity error does not converge to zero. However, convergence rate for the discrete L^2 norm of the velocity error is 1.7. As a test whether the error

in pressure *(i)* is localized around the singularity and *(ii)* converges in some (weighted) norm weaker than L^2 norm we added the last column to the Table 1, which showed 0.5 rate of convergence. The linear regression method has been used to estimate these error reduction rates with respect to the effective mesh size $h_{\text{eff}} = 1/\sqrt{\mathcal{N}(\Omega^h)}$.

6. Conclusions

We developed a new stable MFD method for the Stokes problem. We presented a number of numerical experiments demonstrating the *second-order* convergence for the velocity variable and the *first-order* convergence for the pressure variable. The experiments were done on randomly perturbed quadrilateral, general polygonal and locally refined square meshes and demonstrated method's ability to handle irregular and unstructured meshes.

The new MFD method was derived for tensor viscosity coefficients, thus, allowing to use the method for the problems of linear elasticity in the displacement formulation. The numerical experiments with anisotropic tensor coefficients on unstructured polygonal meshes demonstrated the same order of convergence as in the case of scalar coefficients. The errors were about twice the size of the errors in the case of the scalar coefficients, which is a rather mild effect.

The key difference between the MFD and FE methods is in the definition of the approximation spaces and, henceforth, in the process of constructing mass and stiffness matrices. FE method relies on explicit construction of basis functions for the approximation spaces everywhere inside mesh elements which may require extensive analysis of geometry. MFD method uses only the surface representation of discrete functions. Since no extension inside mesh elements is required, practical implementation of the MFD method is simple for polygonal meshes that may include degenerate and non-convex elements.

Acknowledgments

This work was carried out under the auspices of the National Nuclear Security Administration of the US Department of Energy at Los Alamos National Laboratory under Contract No. DE-AC52-06NA25396 and the DOE Office of Science Advanced Scientific Computing Research (ASCR) Program in Applied Mathematics Research. The work of V. Gyrya was supported in part by DOE Grant DE-FG02-08ER25862 and NSF Grant DMS-0708324.

Appendix A

In Proposition 1 we proved the coercivity of the local bilinear forms $\mathcal{A}_E$ with respect to the seminorm (48). In this section we prove that the local bilinear forms are bounded with respect to the same seminorm, thus showing that a complete equivalence holds. This result, although not fundamental for stability, is important for the convergence of the method and the conditioning of the resulting linear system. We need to start with a preliminary lemma.

Lemma 4. *For all* $V_E \in X_E^h$

$$\min_{\underline{c}\in\mathbb{R}^3} \|V_E + \mathbf{T}_{1..3}\,\underline{c}\| \leqslant C|||V_E|||_{*,E}. \tag{71}$$

Proof. From the definition of the degrees of freedom of $\widetilde{V}_E \in X_E^h$ we have

$$\|\widetilde{V}_E\| \leqslant C\|\tilde{\mathbf{v}}_E\|_{L^\infty(\partial E)}. \tag{72}$$

Since $\boldsymbol{\phi}_1$ and $\boldsymbol{\phi}_3$ span the space of all constant vector fields on E, a simple integration over the edge $e_i \subset \partial E$ gives

$$\min_{c_1,c_3\in\mathbb{R}} \|\tilde{\mathbf{v}}_E + c_1\boldsymbol{\phi}_1 + c_3\boldsymbol{\phi}_3\|^2_{L^\infty(e_i)} \leqslant \left(\int_{e_i}\left|\frac{d}{ds}\tilde{\mathbf{v}}_E(s)\right|ds\right)^2 \leqslant C|e_i|\int_{e_i}\left(\frac{d}{ds}\tilde{\mathbf{v}}_E(s)\right)^2 ds. \tag{73}$$

Combine (72) with (73), taken over all edges $e_i \subset \partial E$, and use the definition of the $|||\cdot|||_E$-norm,

$$\min_{c_1,c_3\in\mathbb{R}} \|\widetilde{V}_E + c_1T_1 + c_3T_3\| \leqslant C\min_{c_1,c_3\in\mathbb{R}} \|\tilde{\mathbf{v}}_E + c_1\boldsymbol{\phi}_1 + c_3\boldsymbol{\phi}_3\|_{L^\infty(\partial E)} \leqslant C\sum_{i=1}^{\mathcal{N}(E)}|e_i|\int_{e_i}\left(\frac{d}{ds}\tilde{\mathbf{v}}_E(s)\right)^2 ds = C|||\widetilde{V}_E|||_E. \tag{74}$$

The result follows from (74) with $\widetilde{V}_E = V_E + c_2T_3$, taking a minimum over c_2, and applying the definition of the $|||\cdot|||_{*,E}$-norm,

$$\min_{\underline{c}\in\mathbb{R}^3} \|V_E + \mathbf{T}_{1..3}\,\underline{c}\| \leqslant \min_{c_2\in\mathbb{R}}\Big(\min_{c_1,c_3\in\mathbb{R}} \|V_E + c_1T_1 + c_2T_2 + c_3T_3\|\Big) \leqslant C\min_{c_2\in\mathbb{R}} |||V_E + c_2T_3|||_E = C|||V_E|||_{\star,E}. \qquad \square$$

Proposition 2. *There exists a positive constant* C_E *(depending only on the tensor* ν *and the geometric constants in Section 4.1.2), such that*

$$\mathcal{A}_E(\mathbf{v}_E,\mathbf{v}_E) = V_E^T\mathbf{A}_E V_E \leqslant C_E|||V_E|||^2_{*,E} \quad \forall V_E \in X_E^h.$$

Proof. Using (54) and the relations (32) and (33) we have

$$\mathbf{R}_E^T V_E = \mathbf{R}_E^T\mathbf{T}_{1..6}\underline{u} + \mathbf{R}_E^T\mathbf{T}_{7..\mathcal{D}}\underline{v} = \widetilde{\mathbf{A}}_E^{11}\underline{u}. \tag{75}$$

First, due to (36) and Lemma 2, then using (75), we obtain

$$\|\underline{u}\|_\star^2 \leqslant C|E|^{-1}\underline{u}^T\widetilde{\mathbf{A}}_E^{11}\underline{u} = C|E|^{-1}\underline{u}^T\mathbf{R}_E^T V_E. \tag{76}$$

Since the first three components of $\mathbf{R}_E^T V_E$ are zeros, using the Cauchy-Schwartz inequality, applied to (76), gives

$$\|\underline{u}\|_\star^2 \leqslant C|E|^{-1}\|\underline{u}\|_\star\|\mathbf{R}_E^T V_E\|_\star \tag{77}$$

which immediately implies

$$\|\underline{u}\|_\star \leqslant C|E|^{-1}\|\mathbf{R}_E^T V_E\|. \tag{78}$$

Due to the mesh assumptions in Section 4.1.2 and the definition in (26), it is easy to check that

$$\|\mathbf{R}_E^T W_E\| \leqslant C|E|^{1/2}\|W_E\| \quad \forall W_E \in X_E^h. \tag{79}$$

Properties (36) and (32) imply that $\mathbf{R}_E^T T_j = 0$ for $j = 1,2,3$. Therefore, applying (79) and afterwards Lemma 4, we get

$$\|\mathbf{R}_E^T V_E\| = \min_{\underline{c}\in\mathbb{R}^3}\|\mathbf{R}_E^T(V_E + \mathbf{T}_{1..3}\underline{c})\| \leqslant C|E|^{1/2}\min_{\underline{c}\in\mathbb{R}^3}\|V_E + \mathbf{T}_{1..3}\underline{c}\| \leqslant C|E|^{1/2}|||V_E|||_{\star,E}. \tag{80}$$

The bounds (78) and (80) give

$$|||V_E|||_{\star,E} \geqslant \beta_E|E|^{1/2}\|\underline{u}\|_\star \tag{81}$$

where β_E is a $|E|$-uniformly positive constant.

Let c_1 and c_2 be two reals, such that $0 < c_1 + c_2 = 1$ (exact definition will follow in (84)). We now write, using (81) and (54) and a triangle inequality,

$$\begin{aligned}|||V_E|||_{\star,E} &= c_1|||V_E|||_{*,E} + c_2|||V_E|||_{\star,E} \geqslant c_1\beta_E|E|^{1/2}\|\underline{u}\|_\star + c_2|||\mathbf{T}_{1..6}\underline{u} + \mathbf{T}_{7..\mathcal{D}}\underline{v}|||_{*,E}.\\ &\geqslant c_1\beta_E|E|^{1/2}\|\underline{u}\|_\star - c_2|||\mathbf{T}_{1..6}\underline{u}|||_{*,E} + c_2|||\mathbf{T}_{7..\mathcal{D}}\underline{v}|||_{*,E}.\end{aligned} \tag{82}$$

From bounds (57) and (82) we infer

$$|||V_E|||_{\star,E} \geqslant (c_1\beta_E - c_2C_*)|E|^{1/2}\|\underline{u}\|_\star + c_2|||\mathbf{T}_{7..\mathcal{D}}\underline{v}|||_{*,E} \tag{83}$$

where by C_* we labeled the square root of the constant in (57). Making the choice

$$c_1 = \frac{1+C_*}{1+\beta_E+C_*} \quad \text{and} \quad c_2 = \frac{\beta_E}{1+\beta_E+C_*}, \tag{84}$$

the bound (83) gives

$$|||V_E|||_{\star,E} \geqslant \alpha'_E(|E|^{1/2}\|\underline{u}\|_\star + |||\mathbf{T}_{7..\mathcal{D}}\underline{v}|||_{*,E}), \tag{85}$$

where $\alpha'_E = \frac{\beta_E}{1+\beta_E+C_*}$ is a $|E|$-uniform positive constant. First, due to (35), then using the orthogonality relation (34) and finally applying Lemma 4, we get

$$|E|^{1/2}\|\underline{v}\| = \|\mathbf{T}_{7..\mathcal{D}}\underline{v}\| = \min_{\underline{c}\in\mathbb{R}^3}\|\mathbf{T}_{7..\mathcal{D}}\underline{v} + \mathbf{T}_{1..3}\underline{c}\| \leqslant C|||\mathbf{T}_{7..\mathcal{D}}\underline{v}|||_{*,E}. \tag{86}$$

The result follows, combining (85), (86) and the equivalence (53). □

References

[1] J.E. Aarnes, S. Krogstad, K.-A. Lie, Multiscale mixed/mimetic methods on corner-point grids, Comp. GeoSci. 12 (3) (2008) 297–315.
[2] L. Beirão da Veiga, A mimetic finite difference method for linear elasticity, Math. Mod. Numer. Anal. (2009), accepted for publication.
[3] L. Beirão da Veiga, A residual based error estimator for the mimetic finite difference method, Numer. Math. 108 (3) (2008) 387–406.
[4] L. Beirão da Veiga, K. Lipnikov, G. Manzini, Convergence analysis of the high-order mimetic finite difference method, Numer. Math. (2009), in press, doi:10.1007/s00211-009-0234-6.
[5] L. Beirão da Veiga, K. Lipnikov, G. Manzini, Convergence of the Mimetic Finite Difference Method for the Stokes Problem on Polyhedral Meshes, IMATI-CNR, Italy, 2009, submitted for publication.
[6] L. Beirão da Veiga, G. Manzini, A higher-order formulation of the mimetic finite difference method, SIAM J. Sci. Comput. 31 (1) (2008) 732–760.
[7] L. Beirao da Veiga, V. Gyrya, K. Lipnikov, V. Manzini, Mimetic Finite Difference Method for the Stokes Problem on Polygonal Meshes, Technical Report LAUR-08-XXXX, Los Alamos National Laboratory, December 2008.
[8] L. Beirao da Veiga, G. Manzini, An a-posteriori error estimator for the mimetic finite difference approximation of elliptic problems, Int. J. Numer. Methods Eng. 76 (11) (2008) 1696–1723.
[9] C. Bernardi, G. Raugel, Méthodes d'éléments finis mixtes pour les équations de Stokes et de Navier–Stokes dans un polygone non convexe, Calcolo 18 (3) (1981) 255–291.
[10] I. Bijelonja, I. Demirdzic, S. Muzaferija, A finite volume method for incompressible linear elasticity, Comput. Meth. Appl. Mech. Eng. 195 (44-47) (2006) 6378–6390.
[11] F. Brezzi, A. Buffa, K. Lipnikov, Mimetic finite differences for elliptic problems, M2AN: Math. Model. Numer. Anal. 43 (2009) 277–295.
[12] F. Brezzi, M. Fortin, Mixed and Hybrid Finite Element Methods, Springer-Verlag, New York, 1991.

[13] F. Brezzi, K. Lipnikov, M. Shashkov, Convergence of the mimetic finite difference method for diffusion problems on polyhedral meshes, SIAM J. Numer. Anal. 43 (5) (2005) 1872–1896.
[14] F. Brezzi, K. Lipnikov, M. Shashkov, V. Simoncini, A new discretization methodology for diffusion problems on generalized polyhedral meshes, Comput. Methods Appl. Mech. Eng. 196 (2007) 3682–3692.
[15] F. Brezzi, K. Lipnikov, V. Simoncini, A family of mimetic finite difference methods on polygonal and polyhedral meshes, Math. Models Methods Appl. Sci. 15 (10) (2005) 1533–1551.
[16] J. Campbell, M. Shashkov, A tensor artificial viscosity using a mimetic finite difference algorithm, J. Comput. Phys. 172 (2001) 739–765.
[17] A. Cangiani, G. Manzini, Flux reconstruction and pressure post-processing in mimetic finite difference methods, Comput. Methods Appl. Mech. Eng. 197/9-12 (2008) 933–945.
[18] A. Cangiani, G. Manzini, A. Russo, Convergence analysis of a mimetic finite difference method for general second-order elliptic problems, SIAM J. Numer. Anal. (2009), in press.
[19] Ph. Clément, Approximation by finite element functions using local regularization, RAIRO Analyse Numérique 9 (R-2) (1975) 77–84.
[20] L. Codecasa, F. Trevisan, Constitutive equations for discrete electromagnetic problems over polyhedral grids, J. Comput. Phys. 225 (2) (2007) 1894–1918.
[21] J. Droniou, R. Eymard, Study of the mixed finite volume method for Stokes and Navier–Stokes equations, Numer. Meth. PDEs 25 (1) (2008) 137–171.
[22] P. Dvorak, New element lops time off CFD simulations, Machine Des. 78 (169) (2006) 154–155.
[23] R. Eymard, T. Gallouët, R. Herbin, A new finite volume scheme for anisotropic diffusion problems on general grids: convergence analysis, C.R. Math. Acad. Sci. Paris 344 (6) (2007) 403–406.
[24] M. Fortin, Old and new finite-elements for incompressible flows, Int. J. Numer. Meth. Fluids 1 (4) (1981) 347–364.
[25] V. Gradinaru, R. Hiptmair, Whitney elements on pyramids, Electron. Trans. Numer. Anal. 8 (1999) 154–168.
[26] V. Gyrya, K. Lipnikov, High-order mimetic finite difference method for diffusion problems on polygonal meshes, J. Comput. Phys. 227 (2008) 8841–8854.
[27] J. Hyman, M. Shashkov, Mimetic discretizations for Maxwell's equations and the equations of magnetic diffusion, Prog. Electromagn. Res. 32 (2001) 89–121.
[28] I.E. Kaporin, High quality preconditioning of a general symmetric positive definite matrix based on its $u^tu + u^tr + r^tu$-decomposition, Numer. Linear Algebra Appl. 5 (6) (1998) 483–509.
[29] Yu. Kuznetsov, S. Repin, New mixed finite element method on polygonal and polyhedral meshes, Russ. J. Numer. Anal. Math. Modell. 18 (3) (2003) 261–278.
[30] S.L. Lyons, R.R. Parashkevov, X.H. Wu, A family of H^1-conforming finite element spaces for calculations on 3D grids with pinch-outs, Numer. Linear Algebra Appl. 13 (9) (2006) 789–799.
[31] L. Margolin, M. Shashkov, P. Smolarkiewicz, A discrete operator calculus for finite difference approximations, Comput. Meth. Appl. Mech. Eng. 187 (2000) 365–383.
[32] J.B. Perot, V. Subramanian, Higher-order mimetic methods for unstructured meshes, J. Comput. Phys. 219 (1) (2006) 68–85.
[33] M. Shashkov, S. Steinberg, Solving diffusion equations with rough coefficients in rough grids, J. Comput. Phys. 129 (1996) 383–405.
[34] K. Stüben, Algebraic multigrid (AMG): experiences and comparisons, Appl. Math. Comput. 13 (1983) 419–452.
[35] A. Tabarraei, N. Sukumar, Application of polygonal finite elements in linear elasticity, Int. J. Comput. Methods 3 (4) (2006) 503–520.
[36] A. Tabarraei, N. Sukumar, Extended finite element method on polygonal and quadtree meshes, Comput. Methods Appl. Mech. Eng. 197 (5) (2007) 425–438.